ETH
Eidgenössische Technische Hochschule Zürich
Swiss Federal Institute of Technology Zurich

Seminar for Applied Mathematics SAM

A fully divergence-free finite element method for magneto-hydrodynamic equations

R. Hiptmair and L.-X. Li and S.-P. Mao and W.-Y. Zheng

Research Report No. 2017-25
May 2017

Seminar für Angewandte Mathematik
Eidgenössische Technische Hochschule
CH-8092 Zürich
Switzerland

Funding: This work is supported in part by the National Center for Mathematics and Interdisciplinary Sciences of China, the State Key Laboratory of Scientific and Engineering Computing of China, and National Magnetic Confinement Fusion Science Program of China (2015GB110003). S. Mao is supported by the National Key Research and Development Program of China (2016YFB0201304), China NSF 11471329, and Youth Innovation Promotion Association of CAS (2016003). W. Zheng is supported by China NSF under the Grant 91430215.

A FULLY DIVERGENCE-FREE FINITE ELEMENT METHOD FOR MAGNETOHYDRODYNAMIC EQUATIONS

RALF HIPTMAIR

Seminar of Applied Mathematics, Swiss Federal Institute of Technology Zurich, CH-8092, Switzerland

ralfh@ethz.ch

LINGXIAO LI

Academy of Mathematics and System Sciences, Chinese Academy of Sciences School of Mathematical Science, University of Chinese Academy of Sciences Beijing, 100190, China

lilingxiao@lsec.cc.ac.cn

SHIPENG MAO

Academy of Mathematics and System Sciences, Chinese Academy of Sciences School of Mathematical Science, University of Chinese Academy of Sciences Beijing, 100190, China

maosp@lsec.cc.ac.cn

WEIYING ZHENG

Academy of Mathematics and System Sciences, Chinese Academy of Sciences School of Mathematical Science, University of Chinese Academy of Sciences Beijing, 100190, China

zwy@lsec.cc.ac.cn

In this paper, a fully divergence-free finite element method is proposed to solve three-dimensional incompressible magnetohydrodynamic equations. The main merit of the method is that the spatial discretization ensures that the approximations of the velocity and the magnetic induction are divergence-free exactly. We employ second-order semi-implicit timestepping, for which we rigorously establish an energy law and, as a consequence, unconditional stability. We prove unique solvability of the linear system of equations to be solved in every timestep. To solve them, we propose an efficient preconditioner so that the number of preconditioned GMRES iterations is uniform with respect to the number of degrees of freedom. Moreover, by several numerical experiments, we confirm the predictions of the theory and demonstrate the efficiency of the preconditioner.

Keywords: Magnetohydrodynamic equations; divergence-free finite element method; preconditioner; magnetic vector potential; driven cavity flow.

AMS Subject Classification: 65M60, 76W05

1. Introduction

The incompressible magnetohydrodynamic (MHD) equations describe the dynamic behavior of an electrically conducting fluid under the influence of a strong magnetic field. They occur in models for, fusion reactor blankets, liquid metal magnetic pumps, aluminum electrolysis among others (see Ref. 1 and 23). MHD is a multiphysics phenomenon: the magnetic field changes the momentum of the fluid through the Lorenz force, and conversely, the conducting fluid influences the magnetic field through electric currents. In this way multiple physical fields, such as the velocity, the pressure, and the electromagnetic fields, are coupled.

In this paper, we study the incompressible MHD equations in a bounded domain $\Omega \subset \mathbb{R}^3$ which consist of the incompressible Navier-Stokes equations and the magnetoquasistatic Maxwell's equations

$$\frac{\partial \boldsymbol{u}}{\partial t} + (\boldsymbol{u}\cdot\nabla)\boldsymbol{u} - \boldsymbol{J}\times\boldsymbol{B} + \nabla p - \nu\Delta\boldsymbol{u} = \boldsymbol{f} \qquad \text{in } \Omega, \tag{1.1a}$$

$$\frac{\partial \boldsymbol{B}}{\partial t} + \mathbf{curl}\,\boldsymbol{E} = 0 \qquad \text{in } \Omega, \tag{1.1b}$$

$$\mathbf{curl}\,\boldsymbol{H} = \boldsymbol{J} \qquad \text{in } \Omega, \tag{1.1c}$$

$$\operatorname{div}\boldsymbol{u} = 0, \qquad \operatorname{div}\boldsymbol{B} = 0 \qquad \text{in } \Omega, \tag{1.1d}$$

where $\boldsymbol{u}$ is the fluid velocity, p is the hydrodynamic pressure, $\boldsymbol{E}$ is the electric field, $\boldsymbol{H}$ is the magnetic field, $\boldsymbol{B}$ is the magnetic induction, $\boldsymbol{J}$ is the electric current density, and $\boldsymbol{f} \in \boldsymbol{L}^2(\Omega)$ stands for the source field. The equations in (1.1) are complemented with the following constitutive equation and Ohm's law

$$\boldsymbol{B} = \mu\boldsymbol{H}, \qquad \boldsymbol{J} = \sigma(\boldsymbol{E} + \boldsymbol{u}\times\boldsymbol{B}). \tag{1.2}$$

The physical parameters are, respectively, the kinematic viscosity ν, the magnetic permeability μ, and the electric conductivity σ. For the well-posedness of (1.1) and (1.2), we assume the following initial and boundary conditions

$$\begin{aligned} &\boldsymbol{u}(0) = \boldsymbol{u}_0,\ \boldsymbol{B}(0) = \boldsymbol{B}_0 \quad \text{in } \Omega, \\ &\boldsymbol{u} = 0, \qquad \boldsymbol{E}\times\boldsymbol{n} = 0 \quad \text{on } \Gamma := \partial\Omega. \end{aligned} \tag{1.3}$$

Numerical methods for incompressible MHD equations has been studied widely. For the stationary model, we refer to Ref. 9, 13, 14, and 27 for stabilized and mixed finite element methods. In Ref. 14, the authors proved optimal error estimates for $\boldsymbol{H}^1(\Omega)$-conforming finite element approximations both to velocity $\boldsymbol{u}$ and magnetic induction $\boldsymbol{B}$ in either polyhedra or domains with $C^{1,1}$-smooth boundaries. It is well-known that $\boldsymbol{B}$ may not be in $\boldsymbol{H}^1(\Omega)$ in general Lipschitz domains which are not convex. In Ref. 27, Schötzau proved the well-posedness of stationary MHD equations and studied a mixed finite element method which discretizes $\boldsymbol{u}$ with $\boldsymbol{H}^1(\Omega)$-conforming finite elements and $\boldsymbol{B}$ with $\boldsymbol{H}(\mathbf{curl},\Omega)$-conforming finite elements. The mixed finite element method yields a discrete magnetic induction $\boldsymbol{B}_h$ which is weakly divergence free, that is, $\boldsymbol{B}_h$ is orthogonal to all discrete gradient fields. In Ref. 12, Greif, Li, Schötzau, and Wei extended the framework by

focusing on the conservation of mass, namely, $\operatorname{div} \boldsymbol{u} = 0$. They proposed a mixed discontinuous Galerkin (DG) finite element method for the stationary MHD model and discretized $\boldsymbol{u}$ in an $\boldsymbol{H}(\operatorname{div}, \Omega)$-conforming finite element space. The merit of the method is that the discrete velocity satisfies $\operatorname{div} \boldsymbol{u}_h = 0$ exactly.

In recent years, exactly divergence-free approximations for $\boldsymbol{B}$ have attracted more and more interests for the spatial discretization of the time-dependent MHD equations, particularly, in the development of a simulation code for fusion reactor blanket (cf. Ref. 1–2). For instance, Ni et al developed current density-conservative finite volume methods for a simplified MHD model on both structured and unstructured grids (cf. Ref. 25, 26, 29, 31). Their methods are efficient for high Hartmann numbers and have been validated by experimental results. In Ref. 18, the authors proposed a stable finite element method for incompressible MHD equations which preserves $\operatorname{div} \boldsymbol{B}_h = 0$ exactly. In contrast to most existing approaches that eliminate the electrical field variable $\boldsymbol{E}$ and give a direct discretization of the magnetic field, they discretizes the electric field $\boldsymbol{E}$ by Nédélec's edge elements and discretizes the magnetic induction $\boldsymbol{B}$ by Raviart-Thomas face elements. In this way, $\operatorname{div} \boldsymbol{B}_h = 0$ is ensured exactly for the discrete solution. In Ref. 19, they also proposed a robust preconditioner for solving the discrete problem.

The purpose of this paper is to propose a new mixed DG finite element method for solving (1.1). Inspired by Ref. 12, we approximate the velocity $\boldsymbol{u}$ by $\boldsymbol{H}(\operatorname{div}, \Omega)$-conforming finite elements and the pressure p by fully discontinuous finite elements. As a result, the conservation of mass is satisfied on the discrete level, that is, $\operatorname{div} \boldsymbol{u}_h = 0$ holds exactly. The divergence-free property of $\boldsymbol{B}$ is realized by means of a magnetic vector potential. Instead of solving for $(\boldsymbol{E}, \boldsymbol{B})$, we solve for the magnetic vector potential $\boldsymbol{A}$ under the temporal gauge so that

$$\boldsymbol{E} = -\frac{\partial \boldsymbol{A}}{\partial t}, \qquad \boldsymbol{B} = \mathbf{curl}\, \boldsymbol{A}.$$

Approximating the vector magnetic potential by $\boldsymbol{H}(\mathbf{curl}, \Omega)$-conforming edge elements and defining $\boldsymbol{B}_h = \mathbf{curl}\, \boldsymbol{A}_h$, we find that $\operatorname{div} \boldsymbol{B}_h = 0$ holds naturally and exactly. We say the mixed finite element method is *fully divergence-free* in the sense that both the discrete velocity and the discrete magnetic induction satisfy exactly

$$\operatorname{div} \boldsymbol{u}_h = 0, \qquad \operatorname{div} \boldsymbol{B}_h = 0.$$

The second objective is to propose an efficient solver for the discrete problem. We propose a linearized discrete problem at t_n by using the extrapolation of the discrete solutions at t_{n-1} and t_{n-2}. We need only solve a linear discrete problem at each time step. Existence and uniqueness of its solution can be shown and a discrete energy law holds for the fully discrete scheme. Numerical experiments show that the extrapolated scheme is second order in time. This means that the proposed method is stable and efficient for long-time simulation of MHD problems.

We also propose a preconditioner for solving the linear systems of equations in each timestep. The optimality of the preconditioner is verified numerically with respect to the number of degrees of freedom (DOFs). Extensive numerical experiments

are presented to verify the convergence rate of the mixed finite element method and the optimality of the preconditioner, to demonstrate the competitive performance of the linear extrapolated scheme, and to validate the $\boldsymbol{A}$-based MHD formulation for an engineering benchmark problem. Furthermore, our numerical results well match the two-dimensional simulations for a driven cavity flow in Ref. 20.

The paper is organized as follows: In Section 2, we introduce the MHD model which uses the velocity, the pressure, and the vector magnetic potential as unknowns. A weak formulation is proposed and the energy law of the solutions is proved. In Section 3, we propose a fully discrete mixed DG finite element method for solving the weak MHD formulation using the extrapolation of the solutions at previous time steps. The energy law of the discrete solutions is also proved under discrete norms. In Section 4, we introduce the preconditioned GMRES algorithm for solving the discrete problem. In Section 5, we present four numerical experiments to confirm the prediction of the theory and to demonstrate the competitive behavior of the MHD solver.

2. A weak formulation of the MHD model

The purpose of this section is to derive a weak formulation of the MHD system (1.1) based on the vector magnetic potential. An energy law for the solutions is also proved. Throughout the paper, we assume that $\Omega \subset \mathbb{R}^3$ is a bounded Lipschitz polyhedral domain with boundary $\Gamma = \partial\Omega$. For simplicity, we assume that the density of fluid $\rho \equiv 1$ and the physical parameters μ, σ, ν are positive constants. Moreover, vector-valued quantities will be denoted by boldface notation, such as $\boldsymbol{L}^2(\Omega) := (L^2(\Omega))^3$.

Let $L^2(\Omega)$ be the space of square-integrable functions and let its inner product and norm be denoted by

$$(u, v) := \int_\Omega uv, \qquad \|u\|_{L^2(\Omega)} := (u, u)^{1/2}.$$

We shall also use the usual Hilbert spaces like $H^1(\Omega)$, $\boldsymbol{H}(\mathbf{curl}, \Omega)$, $\boldsymbol{H}(\mathrm{div}, \Omega)$ and their subspaces $H_0^1(\Omega)$, $\boldsymbol{H}_0(\mathbf{curl}, \Omega)$, $\boldsymbol{H}_0(\mathrm{div}, \Omega)$ with vanishing traces, vanishing tangential traces, and vanishing normal traces on Γ respectively. We refer to Chapter 3 in Ref. 22 for their definitions and inner products. The subsapces of curl-free functions and divergence-free functions are denoted by

$$\begin{aligned} \boldsymbol{H}(\mathrm{div}\, 0, \Omega) &:= \{\boldsymbol{v} \in \boldsymbol{H}(\mathrm{div}, \Omega) \,:\, \mathrm{div}\, \boldsymbol{v} = 0\}, \\ \boldsymbol{H}(\mathbf{curl}\, 0, \Omega) &:= \{\boldsymbol{v} \in \boldsymbol{H}(\mathbf{curl}, \Omega) \,:\, \mathbf{curl}\, \boldsymbol{v} = 0\}. \end{aligned}$$

Since $\mathrm{div}\, \boldsymbol{B} = 0$, we can introduce a magnetic vector potential $\boldsymbol{A}$ and write

$$\boldsymbol{E} = -\partial_t \boldsymbol{A}, \quad \boldsymbol{B} = \mathbf{curl}\, \boldsymbol{A} \quad \text{in } \Omega, \tag{2.1}$$

where the temporal gauge is adopted for convenience. With the abbreviations $\partial_t \boldsymbol{u} =$

$\frac{\partial \boldsymbol{u}}{\partial t}$ and $\partial_t \boldsymbol{A} = \frac{\partial \boldsymbol{A}}{\partial t}$, (1.1) can be written as follows

$$\begin{aligned} \partial_t \boldsymbol{u} + (\boldsymbol{u}\cdot\nabla)\boldsymbol{u} - \boldsymbol{J}\times\mathbf{curl}\,\boldsymbol{A} + \nabla p - \nu\Delta\boldsymbol{u} &= \boldsymbol{f} \quad \text{in } \Omega,\\ \operatorname{div}\boldsymbol{u} &= 0 \quad \text{in } \Omega,\\ \sigma\left(\partial_t\boldsymbol{A} + \mathbf{curl}\,\boldsymbol{A}\times\boldsymbol{u}\right) + \mathbf{curl}\,\mu^{-1}\,\mathbf{curl}\,\boldsymbol{A} &= 0 \quad \text{in } \Omega,\\ -\sigma\left(\partial_t\boldsymbol{A} + \mathbf{curl}\,\boldsymbol{A}\times\boldsymbol{u}\right) &= \boldsymbol{J} \quad \text{in } \Omega. \end{aligned}$$

Using (1.3) and (2.1), it suffices to set the initial condition for $\boldsymbol{A}$ by solving the static problem

$$\begin{aligned} \mathbf{curl}\,\boldsymbol{A}_0 = \boldsymbol{B}_0,\quad \operatorname{div}\boldsymbol{A}_0 = 0 \quad &\text{in } \Omega,\\ \boldsymbol{A}_0\times\boldsymbol{n} = 0 \quad &\text{on } \Gamma. \end{aligned}$$

The boundary condition for $\boldsymbol{A}$ can also be obtained by combining (1.3) and (2.1)

$$\boldsymbol{A}\times\boldsymbol{n} = \boldsymbol{A}_0\times\boldsymbol{n} - \int_0^t (\boldsymbol{E}\times\boldsymbol{n}) = 0 \qquad \text{on } \Gamma.$$

For simplicity, let U_0, B_0, L_0 be the characteristic quantities for velocity, magnetic induction, length of the system respectively. We introduce the following nondimensionalization

$$\boldsymbol{x} \leftarrow \boldsymbol{x}/L_0,\quad t \leftarrow tU_0/L_0,\quad \boldsymbol{A} \leftarrow \boldsymbol{A}/(B_0L_0),\quad \boldsymbol{f} \leftarrow \boldsymbol{f}L_0/U_0^2,\quad p \leftarrow p/U_0^2.$$

The MHD system can be written in a dimensionless form

$$\begin{aligned} \partial_t\boldsymbol{u} + \boldsymbol{u}\cdot\nabla\boldsymbol{u} + \nabla p - R_e^{-1}\Delta\boldsymbol{u} - \kappa\boldsymbol{J}\times\mathbf{curl}\,\boldsymbol{A} &= \boldsymbol{f} \quad \text{in } \Omega, && \text{(2.3a)}\\ \operatorname{div}\boldsymbol{u} &= 0 \quad \text{in } \Omega, && \text{(2.3b)}\\ \partial_t\boldsymbol{A} + \mathbf{curl}\,\boldsymbol{A}\times\boldsymbol{u} + R_m^{-1}\,\mathbf{curl}\,\mathbf{curl}\,\boldsymbol{A} &= 0 \quad \text{in } \Omega, && \text{(2.3c)}\\ -\partial_t\boldsymbol{A} - \mathbf{curl}\,\boldsymbol{A}\times\boldsymbol{u} &= \boldsymbol{J} \quad \text{in } \Omega, && \text{(2.3d)}\\ \boldsymbol{u}(0) = \boldsymbol{u}_0,\quad \boldsymbol{A}(0) &= \boldsymbol{A}_0 \quad \text{in } \Omega, && \text{(2.3e)}\\ \boldsymbol{u} = 0,\quad \boldsymbol{A}\times\boldsymbol{n} &= 0 \quad \text{on } \Gamma, && \text{(2.3f)} \end{aligned}$$

where $R_e = L_0U_0/\nu$ is the Reynolds number, $R_m = \mu\sigma L_0U_0$ is the magnetic Reynolds number, and $\kappa = \sigma B_0^2L_0/U_0$ is the coupling number between the fluid and the magnetic field.

Now we derive a weak formulation of (2.3). For convenience, we introduce some notations for the function spaces

$$\boldsymbol{V} = \boldsymbol{H}_0^1(\Omega)\cap\boldsymbol{H}(\operatorname{div}0,\Omega), \qquad \boldsymbol{C} = \boldsymbol{H}_0(\mathbf{curl},\Omega).$$

Multiply both sides of (2.3a) with $\boldsymbol{v}\in\boldsymbol{V}$. Using integration by part and noting $\boldsymbol{v} = 0$ on Γ, we have

$$(\partial_t\boldsymbol{u} + \boldsymbol{u}\cdot\nabla\boldsymbol{u} - \kappa\boldsymbol{J}\times\mathbf{curl}\,\boldsymbol{A}, \boldsymbol{v}) - (p, \operatorname{div}\boldsymbol{v}) + R_e^{-1}(\nabla\boldsymbol{u}, \nabla\boldsymbol{v}) = (\boldsymbol{f}, \boldsymbol{v}).$$

Using $\operatorname{div}\boldsymbol{v} = 0$ and substituting (2.3d) into the above equality, we get

$$(\partial_t\boldsymbol{u} + \boldsymbol{u}\cdot\nabla\boldsymbol{u}, \boldsymbol{v}) + \kappa(\partial_t\boldsymbol{A} + \mathbf{curl}\,\boldsymbol{A}\times\boldsymbol{u}, \mathbf{curl}\,\boldsymbol{A}\times\boldsymbol{v}) + R_e^{-1}(\nabla\boldsymbol{u}, \nabla\boldsymbol{v}) = (\boldsymbol{f}, \boldsymbol{v}).$$

Similarly, multiplying both sides of (2.3c) with $\boldsymbol{\varphi} \in \boldsymbol{C}$, using integration by part, and noting $\boldsymbol{\varphi} \times \boldsymbol{n} = 0$, we have

$$(\partial_t \boldsymbol{A} + \mathbf{curl}\, \boldsymbol{A} \times \boldsymbol{u}, \boldsymbol{\varphi}) + R_m^{-1}(\mathbf{curl}\, \boldsymbol{A}, \mathbf{curl}\, \boldsymbol{\varphi}) = 0.$$

Then we get a weak formulation of (2.3): Find $\boldsymbol{u} \in \boldsymbol{V}$, $\boldsymbol{A} \in \boldsymbol{C}$ such that $\boldsymbol{A}(0) = \boldsymbol{A}_0$, $\boldsymbol{u}(0) = \boldsymbol{u}_0$, and

$$(\partial_t \boldsymbol{u}, \boldsymbol{v}) + \mathcal{O}(\boldsymbol{u}; \boldsymbol{u}, \boldsymbol{v}) + \mathcal{A}(\boldsymbol{u}, \boldsymbol{v}) + \kappa(\partial_t \boldsymbol{A} + \boldsymbol{B} \times \boldsymbol{u}, \boldsymbol{B} \times \boldsymbol{v}) = (\boldsymbol{f}, \boldsymbol{v}) \quad \forall \boldsymbol{v} \in \boldsymbol{V}, \tag{2.4a}$$

$$(\partial_t \boldsymbol{A} + \boldsymbol{B} \times \boldsymbol{u}, \boldsymbol{\varphi}) + R_m^{-1}(\mathbf{curl}\, \boldsymbol{A}, \mathbf{curl}\, \boldsymbol{\varphi}) = 0 \quad \forall \boldsymbol{\varphi} \in \boldsymbol{C}, \tag{2.4b}$$

where $\boldsymbol{B} = \mathbf{curl}\, \boldsymbol{A}$ and

$$\mathcal{O}(\boldsymbol{w}; \boldsymbol{u}, \boldsymbol{v}) = ((\boldsymbol{w} \cdot \nabla)\boldsymbol{u}, \boldsymbol{v}), \qquad \mathcal{A}(\boldsymbol{v}, \boldsymbol{w}) = R_e^{-1}(\nabla \boldsymbol{v}, \nabla \boldsymbol{w}).$$

Using (2.3a), the pressure can be recovered by solving the Poisson equation: Find $p \in H^1(\Omega)/\mathbb{R}$ such that

$$(\nabla p, \nabla q) = (\boldsymbol{f} + \boldsymbol{J} \times \mathbf{curl}\, \boldsymbol{A}, \nabla q) - \mathcal{O}(\boldsymbol{u}; \boldsymbol{u}, \nabla q) \qquad \forall\, q \in H^1(\Omega)/\mathbb{R}. \tag{2.5}$$

Theorem 2.1. *Let $\boldsymbol{u}$, $\boldsymbol{A}$ be the solutions of (2.4) and assume*

$$\begin{aligned} &\boldsymbol{u} \in \boldsymbol{L}^\infty(0, T; \boldsymbol{L}^2(\Omega)) \cap \boldsymbol{L}^2(0, T; \boldsymbol{V}), \\ &\boldsymbol{A} \in \boldsymbol{H}^1(0, T; \boldsymbol{L}^2(\Omega)) \cap \boldsymbol{L}^\infty(0, T; \boldsymbol{C}), \\ &\boldsymbol{J} \in \boldsymbol{L}^2(0, T; \boldsymbol{L}^2(\Omega)). \end{aligned}$$

Then the energy law holds

$$\mathsf{E}(T) + \int_0^T \mathsf{P}(t)\mathrm{d}t = \mathsf{E}(0) + \int_0^T (\boldsymbol{f}, \boldsymbol{u}),$$

where

$$\mathsf{E}(t) := \frac{1}{2} \|\boldsymbol{u}\|^2_{\boldsymbol{L}^2(\Omega)} + \frac{\kappa}{2R_m} \|\boldsymbol{B}\|^2_{\boldsymbol{L}^2(\Omega)}, \quad \mathsf{P}(t) := \frac{1}{R_e} \|\nabla \boldsymbol{u}\|^2_{\boldsymbol{L}^2(\Omega)} + \kappa \|\boldsymbol{J}\|^2_{\boldsymbol{L}^2(\Omega)}.$$

Proof. For any $\boldsymbol{w} \in \boldsymbol{V}$, since $\operatorname{div} \boldsymbol{w} = 0$, direct calculations show that

$$\int_\Omega (\boldsymbol{w} \cdot \nabla)\boldsymbol{u} \cdot \boldsymbol{v} = -\int_\Omega (\boldsymbol{w} \cdot \nabla)\boldsymbol{v} \cdot \boldsymbol{u} \qquad \forall\, \boldsymbol{v} \in \boldsymbol{H}^1_0(\Omega).$$

This means that $\mathcal{O}(\boldsymbol{w}; \boldsymbol{u}, \boldsymbol{u}) = 0$. Since $\partial_t \boldsymbol{A}, \boldsymbol{J} \in \boldsymbol{L}^2(0, T; \boldsymbol{L}^2(\Omega))$, we have $\boldsymbol{B} \times \boldsymbol{u} \in \boldsymbol{L}^2(0, T; \boldsymbol{L}^2(\Omega))$. Taking $\boldsymbol{v} = \boldsymbol{u}$ in (2.4a) shows that

$$\frac{1}{2} \frac{\mathrm{d}}{\mathrm{d}t} \|\boldsymbol{u}\|^2_{\boldsymbol{L}^2(\Omega)} - \kappa(\boldsymbol{J}, \boldsymbol{B} \times \boldsymbol{u}) + \frac{1}{R_e} \|\nabla \boldsymbol{u}\|^2_{\boldsymbol{L}^2(\Omega)} = (\boldsymbol{f}, \boldsymbol{u}). \tag{2.6}$$

Furthermore, taking $\boldsymbol{\varphi} = \partial_t \boldsymbol{A}$ in (2.4b), we also have

$$\frac{1}{2R_m} \frac{\mathrm{d}}{\mathrm{d}t} \|\boldsymbol{B}\|^2_{\boldsymbol{L}^2(\Omega)} = (\boldsymbol{J}, \partial_t \boldsymbol{A}) = -\|\boldsymbol{J}\|^2_{\boldsymbol{L}^2(\Omega)} - (\boldsymbol{J}, \boldsymbol{B} \times \boldsymbol{u}). \tag{2.7}$$

Substituting (2.7) into (2.6) yields the result. □

Remark 2.1. The energy law describes the variation of the total energy caused by energy transformation and the work of external forces. The total energy E consists of the fluid kinetic energy $\frac{1}{2}\|\boldsymbol{u}\|^2_{\boldsymbol{L}^2(\Omega)}$ and the magnetic field energy $\frac{\kappa}{2R_m}\|\boldsymbol{B}\|^2_{\boldsymbol{L}^2(\Omega)}$. The dissipation of the total energy stems from the friction losses $R_e^{-1}\|\nabla\boldsymbol{u}\|^2_{\boldsymbol{L}^2(\Omega)}$ and the Ohmic losses $\kappa\|\boldsymbol{J}\|^2_{\boldsymbol{L}^2(\Omega)}$. The energy supply from external sources is represented by $(\boldsymbol{f},\boldsymbol{u})$.

3. An interior-penalty finite element method

In this section, we study the fully discrete approximation to the MHD equations. The velocity $\boldsymbol{u}$ shall be discretized by $\boldsymbol{H}(\mathrm{div},\Omega)$-conforming finite elements with interior penalties in a DG-type approach. We refer to Ref. 12 for the interior-penalty finite element method for the $\boldsymbol{H}$-based formulation of stationary MHD model.

3.1. *Finite element spaces*

Let $\mathcal{T}_h$ be a shape-regular tetrahedral triangulation of Ω and let $\mathcal{F}_h$ be the set of all element faces of $\mathcal{T}_h$. The $H_0^1(\Omega)$-conforming finite element space of piecewise quadratic polynomials is defined by

$$U_h = \{v \in H_0^1(\Omega) : v|_K \in P_2(K),\ K \in \mathcal{T}_h\},$$

where $P_k(K)$ is the space of polynomials with degrees no more than $k \geq 0$. We also use the notation $\boldsymbol{P}_k(K) = P_k(K)^3$. The linear $\boldsymbol{H}_0(\mathrm{div},\Omega)$- and $\boldsymbol{H}_0(\mathbf{curl},\Omega)$-conforming finite element spaces are defined respectively as follows (c.f. Ref. 24, 28):

$$\boldsymbol{V}_h = \{\boldsymbol{v} \in \boldsymbol{H}_0(\mathrm{div},\Omega) : \boldsymbol{v}|_K \in \boldsymbol{P}_1(K),\ K \in \mathcal{T}_h\},$$
$$\boldsymbol{C}_h = \{\boldsymbol{v} \in \boldsymbol{H}_0(\mathbf{curl},\Omega) : \boldsymbol{v}|_K \in \boldsymbol{P}_1(K),\ K \in \mathcal{T}_h\}.$$

For convenience, we denote the divergence-free subspace of $\boldsymbol{V}_h$ as follows

$$\boldsymbol{V}_h(\mathrm{div}\,0) := \boldsymbol{V}_h \cap \boldsymbol{H}(\mathrm{div}\,0,\Omega).$$

Now we introduce the notations associated with traces. We endow each $F \in \mathcal{F}_h$ with a unit normal $\boldsymbol{n}_F$ which points to the exterior of Ω when $F \subset \Gamma$. For any interior face $F \in \mathcal{F}_h$, let K_+, K_- be two adjacent elements of $\mathcal{T}_h$ such that $F = \partial K_+ \cap K_- \in \mathcal{F}_h$. We always assume that $\boldsymbol{n}_F$ points to the exterior of K_+. Let φ be a scalar-, vector-, or matrix-valued function which is piecewise smooth over $\mathcal{T}_h$. The mean value and jump of φ on F are defined respectively by

$$\{\!\{\varphi\}\!\} := \frac{1}{2}(\varphi_+ + \varphi_-), \quad [\![\varphi]\!] := \varphi_+ - \varphi_- \quad \text{on } F,$$

where $\varphi_\pm$ denote the traces of φ on F from inside of $K_\pm$ respectively. For any face $F = \partial K_+ \cap \Gamma$ with $K_+ \in \mathcal{T}_h$, the mean value and the jump of φ on F are defined by

$$\{\!\{\varphi\}\!\} = [\![\varphi]\!] = \varphi_+ \quad \text{on } F,$$

We shall use the discrete semi-norm and norms

$$\|\boldsymbol{u}\|_{0,h} := \left(\sum_{F\in\mathcal{F}_h} h_F^{-1} \|\boldsymbol{u}\|^2_{\boldsymbol{L}^2(F)} \right)^{\frac{1}{2}}, \qquad |\boldsymbol{u}|_{1,h} := \left(\sum_{K\in\mathcal{T}_h} \|\nabla \boldsymbol{u}\|^2_{\boldsymbol{L}^2(K)} \right)^{\frac{1}{2}},$$
$$\|\boldsymbol{u}\|_{1,h} := \left(|\boldsymbol{u}|^2_{1,h} + \|[\![\boldsymbol{u}]\!]\|^2_{0,h} \right)^{\frac{1}{2}}.$$

We shall also use the space of piecewise regular functions

$$\boldsymbol{H}^1(\mathcal{T}_h) := \left\{ \boldsymbol{v} \in \boldsymbol{L}^2(\Omega) : \ \boldsymbol{v}|_K \in \boldsymbol{H}^1(K), \ \ K \in \mathcal{T}_h \right\},$$
$$\boldsymbol{V}(h) := \boldsymbol{V} + \boldsymbol{V}_h .$$

Apparently the embedding relationship holds

$$\boldsymbol{V}(h) \subset \boldsymbol{H}^1(\Omega) + \boldsymbol{V}_h \subset \boldsymbol{H}^1(\mathcal{T}_h).$$

Lemma 3.1. *For any $2 \le p \le 6$, there exists a constant $C(p) > 0$ independent of the mesh size such that*

$$\|\boldsymbol{v}\|_{\boldsymbol{L}^p(\Omega)} \le C(p) \|\boldsymbol{v}\|_{1,h} \qquad \forall\, \boldsymbol{v} \in \boldsymbol{V}(h) . \tag{3.1}$$

Proof. The inequality is proved for two-dimensional case in Lemma 6.2 of Ref. 11. In fact, a careful inspection of its proof shows that it also applies to three-dimensional case. We do not elaborate on the details. For $p = 2$, we also refer to Ref. 4 and 6. □

The discrete counterparts of the bilinear and trilinear forms are defined by

$$\mathcal{A}_h(\boldsymbol{v}, \boldsymbol{w}) = \frac{1}{R_e} \sum_{K\in\mathcal{T}_h} \int_K \nabla \boldsymbol{v} : \nabla \boldsymbol{w} + \frac{\alpha}{R_e} \sum_{F\in\mathcal{F}_h} h_F^{-1} \int_F [\![\boldsymbol{u}]\!] \cdot [\![\boldsymbol{v}]\!]$$
$$- \frac{1}{R_e} \sum_{F\in\mathcal{F}_h} \int_F \left(\left\{\!\!\left\{ \frac{\partial \boldsymbol{u}}{\partial \boldsymbol{n}} \right\}\!\!\right\} \cdot [\![\boldsymbol{v}]\!] + \left\{\!\!\left\{ \frac{\partial \boldsymbol{v}}{\partial \boldsymbol{n}} \right\}\!\!\right\} \cdot [\![\boldsymbol{u}]\!] \right),$$
$$O_h(\boldsymbol{w}; \boldsymbol{u}, \boldsymbol{v}) = - \sum_{K\in\mathcal{T}_h} \int_K \boldsymbol{u} \cdot \operatorname{div}(\boldsymbol{w} \otimes \boldsymbol{v}) + \sum_{K\in\mathcal{T}_h} \int_{\partial K} (\boldsymbol{w} \cdot \boldsymbol{n}_K) \left(\boldsymbol{u}^{\downarrow} \cdot \boldsymbol{v} \right),$$

where $\alpha > 0$ is the penalty parameter independent of the mesh, $\boldsymbol{n}_K$ is the unit outer normal of ∂K, $\boldsymbol{n}_F$ is the unit normal of n_F, and $\boldsymbol{u}^{\downarrow}$ denotes the upwind convective flux defined by Ref. 8, 12

$$\boldsymbol{u}^{\downarrow}(\boldsymbol{x}) = \begin{cases} \lim\limits_{\varepsilon\to 0+} \boldsymbol{u}(\boldsymbol{x} - \varepsilon \boldsymbol{w}(x)), & \boldsymbol{x} \in \partial K \backslash \Gamma, \\ 0, & \boldsymbol{x} \in \partial K \cap \Gamma. \end{cases}$$

The following lemma states that the discrete bilinear form $\mathcal{A}_h(\cdot,\cdot)$ is coercive on $\boldsymbol{V}_h$.

Lemma 3.2. *Suppose α is large enough but independent of h_F, R_e, and R_m. Then there exists a constant $\theta_1 > 0$ independent of h_F, R_e, and R_m such that*

$$\mathcal{A}_h(\boldsymbol{v}_h, \boldsymbol{v}_h) \geq \frac{\theta_1}{R_e} \|\boldsymbol{v}_h\|_{1,h}^2 \qquad \forall\, \boldsymbol{v} \in \boldsymbol{V}_h.$$

Proof. The proof is standard. We present it here for completeness. By the norm equivalence on finite dimensional space (cf. Lemma A.6 in Ref. 11), there exists a constant C_1 independent of h such that

$$h_F \|\nabla \boldsymbol{v}_h\|_{\boldsymbol{L}^2(F)}^2 \leq C_1 \|\nabla \boldsymbol{v}_h\|_{\boldsymbol{L}^2(K_F)}^2 \qquad \forall\, F \in \mathcal{F}_h,$$

where $K_F \in \mathcal{T}_h$ satisfies $F \subset \partial K_F$. Therefore

$$\begin{aligned} R_e \mathcal{A}_h(\boldsymbol{v}, \boldsymbol{v}) &= |\boldsymbol{v}|_{1,h}^2 + \alpha \|[\![\boldsymbol{v}]\!]\|_{0,h}^2 - 2 \sum_{F \in \mathcal{F}_h} \int_F \left\{\!\!\left\{ \frac{\partial \boldsymbol{v}}{\partial \boldsymbol{n}} \right\}\!\!\right\} \cdot [\![\boldsymbol{v}]\!] \\ &\geq |\boldsymbol{v}|_{1,h}^2 + (\alpha - 2C_1^2) \|[\![\boldsymbol{v}]\!]\|_{0,h}^2 - \frac{1}{2C_1} \sum_{F \in \mathcal{F}_h} h_F \|\{\!\{\nabla \boldsymbol{v}\}\!\}\|_{\boldsymbol{L}^2(F)}^2 \\ &\geq \frac{1}{2} |\boldsymbol{v}|_{1,h}^2 + (\alpha - 2C_1^2) \|[\![\boldsymbol{v}]\!]\|_{0,h}^2 . \end{aligned}$$

We complete the proof by setting $\alpha > 2C_1^2$ and $\theta_1 := \min(1/2, \alpha - 2C_1^2)$. □

Lemma 3.2 states that $\mathcal{A}_h(\cdot,\cdot)$ is coercive on $\boldsymbol{H}^1(\mathcal{T}_h)$. It forms an equivalent norm

$$\|\boldsymbol{v}\|_{\mathcal{A}_h} := \sqrt{\mathcal{A}_h(\boldsymbol{v}, \boldsymbol{v})} \qquad \forall\, \boldsymbol{v} \in \boldsymbol{H}^1(\mathcal{T}_h).$$

We cite Ref. 8 for the following lemma on the positivity and continuity of the trilinear form $\mathcal{O}$. The proof is omitted here.

Lemma 3.3. *Let $\boldsymbol{w}, \boldsymbol{w}_1 \in \boldsymbol{H}^1(\mathcal{T}_h) \cap \boldsymbol{H}(\operatorname{div} 0, \Omega)$, $\boldsymbol{u} \in \boldsymbol{V}(h)$, and $\boldsymbol{v} \in \boldsymbol{V}_h$. Then*

$$\mathcal{O}_h(\boldsymbol{w}; \boldsymbol{v}, \boldsymbol{v}) = \frac{1}{2} \sum_{F \in \mathcal{F}_h} \int_F |\boldsymbol{w} \cdot \boldsymbol{n}| \, |[\![\boldsymbol{v}]\!]|^2 \ .$$

Furthermore, there exists a constant C_0 independent of the mesh size such that

$$|\mathcal{O}(\boldsymbol{w}; \boldsymbol{u}, \boldsymbol{v}) - \mathcal{O}(\boldsymbol{w}_1; \boldsymbol{u}, \boldsymbol{v})| \leq C_0 \|\boldsymbol{w} - \boldsymbol{w}_1\|_{1,h} \|\boldsymbol{u}\|_{1,h} \|\boldsymbol{v}\|_{1,h} \ .$$

3.2. *A semi-implicit time-stepping scheme*

Now we study the fully discrete approximation to the MHD equations. Let $\{t_n = n\tau : \ n = 0, 1, \cdots, N\}$, $\tau = T/N$, be an equidistant partition of the time interval $[0, T]$. For a sequence of functions $\{\boldsymbol{v}_n\}$, we define the finite difference operator and mean values by

$$\begin{aligned} &\delta_t \boldsymbol{v}_n := \frac{\boldsymbol{v}_n - \boldsymbol{v}_{n-1}}{\tau}, \qquad \bar{\boldsymbol{v}}_n := \frac{\boldsymbol{v}_n + \boldsymbol{v}_{n-1}}{2}, \\ &\boldsymbol{f}_n := \frac{1}{6} \left[\boldsymbol{f}(t_n) + 4\boldsymbol{f}(t_{n-1/2}) + \boldsymbol{f}(t_{n-1}) \right]. \end{aligned} \tag{3.2}$$

Let $\boldsymbol{u}_0^h$, $\boldsymbol{A}_0^h$ be quasi-interpolations of the initial conditions $\boldsymbol{u}_0 \in \boldsymbol{H}_0^1(\Omega)$, $\boldsymbol{A}_0 \in \boldsymbol{H}_0(\mathbf{curl}, \Omega)$ onto the finite element spaces $\boldsymbol{V}_h$ and $\boldsymbol{C}_h$ respectively (cf. e.g. Ref. 17). Without causing confusion, we shall drop the superscripts and denote by $\boldsymbol{u}_0 \in \boldsymbol{V}_h$, $\boldsymbol{A}_0 \in \boldsymbol{C}_h$ the discrete initial values.

The Crank-Nicolson scheme for the fully discrete approximation of (2.4) reads: Find $(\boldsymbol{u}_n, \boldsymbol{A}_n) \in \boldsymbol{V}_h(\operatorname{div} 0) \times \boldsymbol{C}_h$, $n \geq 0$, such that

$$(\delta_t \boldsymbol{u}_n, \boldsymbol{v}) + \mathcal{O}_h(\bar{\boldsymbol{u}}_n; \bar{\boldsymbol{u}}_n, \boldsymbol{v}) + \mathcal{A}_h(\bar{\boldsymbol{u}}_n, \boldsymbol{v}) + \kappa(\delta_t \boldsymbol{A}_n + \bar{\boldsymbol{B}}_n \times \bar{\boldsymbol{u}}_n, \bar{\boldsymbol{B}}_n \times \boldsymbol{v}) = (\boldsymbol{f}_n, \boldsymbol{v}), \tag{3.3a}$$

$$\big(\delta_t \boldsymbol{A}_n + \bar{\boldsymbol{B}}_n \times \bar{\boldsymbol{u}}_n, \boldsymbol{\varphi}\big) + R_m^{-1}(\mathbf{curl}\, \bar{\boldsymbol{A}}_n, \mathbf{curl}\, \boldsymbol{\varphi}) = 0, \tag{3.3b}$$

for all $(\boldsymbol{v}, \boldsymbol{\varphi}) \in \boldsymbol{V}_h(\operatorname{div} 0) \times \boldsymbol{C}_h$, where $\bar{\boldsymbol{B}}_n = \mathbf{curl}\, \bar{\boldsymbol{A}}_n$. It is well-known that the Crank-Nicolson scheme is of second order with respect to τ. The discrete problem is nonlinear and expensive to solve at each time step. Thus, inspired by Ref. 3 and 30, we consider the linearly extrapolated solutions

$$\boldsymbol{u}_* = \frac{1}{2}(3\boldsymbol{u}_{n-1} - \boldsymbol{u}_{n-2}), \quad \boldsymbol{B}_* = \frac{1}{2}(3\boldsymbol{B}_{n-1} - \boldsymbol{B}_{n-2}) = \frac{1}{2}\,\mathbf{curl}(3\boldsymbol{A}_{n-1} - \boldsymbol{A}_{n-2}). \tag{3.4}$$

The truncation errors for the above approximations are of second order. For any smooth function v, let $\bar{v}_n = [v(t_n) + v(t_{n-1})]/2$ and $v_* = [3v(t_{n-1}) - v(t_{n-2})]/2$. Then

$$v_* - \bar{v}_n = \frac{1}{2}[v(t_{n-2}) + v(t_n) - 2v(t_{n-1})] = v_{tt}(t_{n-1})\tau^2 + O(\tau^3). \tag{3.5}$$

Linearize the nonlinear terms in (3.3) by replacing $\bar{\boldsymbol{u}}_n, \bar{\boldsymbol{B}}_n$ with $\boldsymbol{u}_*$, $\boldsymbol{B}_*$ for $n \geq 2$ and with $\boldsymbol{u}_0$, $\boldsymbol{A}_0$ for $n = 1$. We get the semi-implicit time-stepping scheme for (2.4):

Find $(\boldsymbol{u}_n, \boldsymbol{A}_n) \in \boldsymbol{V}_h(\operatorname{div} 0) \times \boldsymbol{C}_h$, $n \geq 2$, such that, for any $(\boldsymbol{v}, \boldsymbol{\varphi}) \in \boldsymbol{V}_h(\operatorname{div} 0) \times \boldsymbol{C}_h$,

$$(\delta_t \boldsymbol{u}_n, \boldsymbol{v}) + \mathcal{O}_h(\boldsymbol{u}_*; \bar{\boldsymbol{u}}_n, \boldsymbol{v}) + \mathcal{A}_h(\bar{\boldsymbol{u}}_n, \boldsymbol{v}) + \kappa(\delta_t \boldsymbol{A}_n + \boldsymbol{B}_* \times \bar{\boldsymbol{u}}_n, \boldsymbol{B}_* \times \boldsymbol{v}) = (\boldsymbol{f}_n, \boldsymbol{v}), \tag{3.6a}$$

$$(\delta_t \boldsymbol{A}_n + \boldsymbol{B}_* \times \bar{\boldsymbol{u}}_n, \boldsymbol{\varphi}) + \frac{1}{R_m}(\mathbf{curl}\, \bar{\boldsymbol{A}}_n, \mathbf{curl}\, \boldsymbol{\varphi}) = 0. \tag{3.6b}$$

Theorem 3.1. *The discrete problem* (3.6) *has a unique solution in each time step. The discrete energy law holds*

$$\frac{\mathsf{E}_n - \mathsf{E}_{n-1}}{\tau} + \mathsf{P}_n = (\boldsymbol{f}_n, \bar{\boldsymbol{u}}_n) \qquad \forall\, n \geq 1, \tag{3.7}$$

where

$$\mathsf{E}_n := \frac{1}{2}\left\|\boldsymbol{u}_n\right\|^2_{\boldsymbol{L}^2(\Omega)} + \frac{\kappa}{2R_m}\left\|\mathbf{curl}\,\boldsymbol{A}_n\right\|^2_{\boldsymbol{L}^2(\Omega)},$$

$$\mathsf{P}_n := \left\|\bar{\boldsymbol{u}}_n\right\|^2_{\mathcal{A}_h} + \frac{1}{2}\sum_{F\in\mathcal{F}_h}\int_F |\boldsymbol{u}_*\cdot\boldsymbol{n}|\left|[\![\bar{\boldsymbol{u}}_n]\!]\right|^2 + \kappa\left\|\delta_t\boldsymbol{A}_n + \boldsymbol{B}_*\times\bar{\boldsymbol{u}}_n\right\|^2_{\boldsymbol{L}^2(\Omega)}.$$

Proof. We first prove the discrete energy law. Let $\boldsymbol{J}_n := -\delta_t\boldsymbol{A}_n - \boldsymbol{B}_*\times\bar{\boldsymbol{u}}_n$ be the discrete electric current density. Taking $\boldsymbol{v} = \bar{\boldsymbol{u}}_n$ in (3.6a) yields

$$(\delta_t\boldsymbol{u}_n, \bar{\boldsymbol{u}}_n) + \mathcal{O}_h(\boldsymbol{u}_*; \bar{\boldsymbol{u}}_n, \bar{\boldsymbol{u}}_n) + \mathcal{A}_h(\bar{\boldsymbol{u}}_n, \bar{\boldsymbol{u}}_n) = \kappa\,(\boldsymbol{J}_n, \boldsymbol{B}_*\times\bar{\boldsymbol{u}}_n) + (\boldsymbol{f}_n, \bar{\boldsymbol{u}}_n). \tag{3.8}$$

Since $\bar{\boldsymbol{u}}_n \in \boldsymbol{V}_h \cap \boldsymbol{H}(\operatorname{div}0,\Omega)$, from Lemma 3.3 we have

$$O_h(\boldsymbol{u}_*; \bar{\boldsymbol{u}}_n, \bar{\boldsymbol{u}}_n) = \frac{1}{2}\sum_{F\in\mathcal{F}_h}\int_F |\boldsymbol{u}_*\cdot\boldsymbol{n}|\left|[\![\bar{\boldsymbol{u}}_n]\!]\right|^2 .$$

Furthermore, by taking $\boldsymbol{\varphi} = \delta_t\boldsymbol{A}_n$ in (3.6b), we find that

$$\frac{1}{R_m}\left(\mathbf{curl}\,\bar{\boldsymbol{A}}_n, \mathbf{curl}\,\delta_t\boldsymbol{A}_n\right) = (\boldsymbol{J}_n, \delta_t\boldsymbol{A}_n) = -(\boldsymbol{J}_n, \boldsymbol{B}_*\times\bar{\boldsymbol{u}}_n) - \kappa^{-1}\left\|\boldsymbol{J}_n\right\|^2_{\boldsymbol{L}^2(\Omega)}.$$

It follows that

$$(\boldsymbol{J}_n, \boldsymbol{B}_*\times\bar{\boldsymbol{u}}_n) = -\kappa^{-1}\left\|\boldsymbol{J}_n\right\|^2_{\boldsymbol{L}^2(\Omega)} - \frac{1}{R_m}\left(\mathbf{curl}\,\bar{\boldsymbol{A}}_n, \mathbf{curl}\,\delta_t\boldsymbol{A}_n\right). \tag{3.9}$$

By direct calculations, we obtain the identities

$$(\delta_t\boldsymbol{u}_n, \bar{\boldsymbol{u}}_n) = \frac{1}{2\tau}\left(\left\|\boldsymbol{u}_n\right\|^2_{\boldsymbol{L}^2(\Omega)} - \left\|\boldsymbol{u}_{n-1}\right\|^2_{\boldsymbol{L}^2(\Omega)}\right),$$

$$\left(\mathbf{curl}\,\bar{\boldsymbol{A}}_n, \mathbf{curl}\,\delta_t\boldsymbol{A}_n\right) = \frac{1}{2\tau}\left(\left\|\mathbf{curl}\,\boldsymbol{A}_n\right\|^2_{\boldsymbol{L}^2(\Omega)} - \left\|\mathbf{curl}\,\boldsymbol{A}_{n-1}\right\|^2_{\boldsymbol{L}^2(\Omega)}\right).$$

Inserting (3.9) into (3.8) yields (3.7).

To prove the well-posedness of (3.6), we write $\bar{\boldsymbol{\Psi}}_n = (\bar{\boldsymbol{u}}_n, \bar{\boldsymbol{A}}_n)$ and consider an equivalent form of (3.6): Find $\bar{\boldsymbol{\Psi}}_n \in \boldsymbol{V}_h(\operatorname{div}0)\times\boldsymbol{C}_h$ such that

$$a(\bar{\boldsymbol{\Psi}}_n, \boldsymbol{\Phi}) = f(\boldsymbol{\Phi}) \qquad \forall\,\boldsymbol{\Phi} \in \boldsymbol{V}_h(\operatorname{div}0)\times\boldsymbol{C}_h. \tag{3.10}$$

For any $\boldsymbol{\Psi} = (\boldsymbol{u}, \boldsymbol{A})$, $\boldsymbol{\Phi} = (\boldsymbol{v}, \boldsymbol{\varphi})$ with $\boldsymbol{u}, \boldsymbol{v} \in \boldsymbol{V}_h(\operatorname{div}0)$ and $\boldsymbol{A}, \boldsymbol{\varphi} \in \boldsymbol{C}_h$, the bilinear

form and the right-hand side are defined by

$$\begin{aligned} a(\boldsymbol{\Psi},\boldsymbol{\Phi}) &:= \frac{2}{\tau}\left(\boldsymbol{u},\boldsymbol{v}\right) + \mathcal{O}_h(\boldsymbol{u}_*;\boldsymbol{u},\boldsymbol{v}) + \mathcal{A}_h(\boldsymbol{u},\boldsymbol{v}) + \frac{2\kappa}{\tau R_m}(\mathbf{curl}\,\boldsymbol{A},\mathbf{curl}\,\boldsymbol{\varphi}) \\ &\quad +\kappa\left(\frac{2}{\tau}\boldsymbol{A}+\boldsymbol{B}_*\times\boldsymbol{u},\frac{2}{\tau}\boldsymbol{\varphi}+\boldsymbol{B}_*\times\boldsymbol{v}\right), \\ f(\boldsymbol{\Phi}) &:= \left(\boldsymbol{f}_n+\frac{2}{\tau}\boldsymbol{u}_{n-1},\boldsymbol{v}\right)+\kappa\left(\frac{2}{\tau}\boldsymbol{A}_{n-1},\frac{2}{\tau}\boldsymbol{\varphi}+\boldsymbol{B}_*\times\boldsymbol{v}\right). \end{aligned}$$

It is easy to see that

$$|||\boldsymbol{\Phi}||| = \left(\frac{2}{\tau}\left\|\boldsymbol{v}\right\|^2_{\boldsymbol{L}^2(\Omega)} + \left\|\boldsymbol{v}\right\|^2_{\mathcal{A}_h} + \frac{2\kappa}{\tau R_m}\left\|\mathbf{curl}\,\boldsymbol{\varphi}\right\|^2_{\boldsymbol{L}^2(\Omega)} + \kappa\left\|\frac{2}{\tau}\boldsymbol{\varphi}+\boldsymbol{B}_*\times\boldsymbol{v}\right\|^2_{\boldsymbol{L}^2(\Omega)}\right)^{\frac{1}{2}}$$

provides a norm on $\boldsymbol{V}_h(\operatorname{div}0)\times\boldsymbol{C}_h$. From Lemma 3.3, $\mathcal{O}_h\big(\boldsymbol{u}_*;\boldsymbol{v},\boldsymbol{v}\big)\geq 0$ and

$$a(\boldsymbol{\Phi},\boldsymbol{\Phi}) \geq |||\boldsymbol{\Phi}|||^2 \qquad \forall\,\boldsymbol{\Phi}\in\boldsymbol{V}_h(\operatorname{div}0)\times\boldsymbol{C}_h\,.$$

Therefore, the bilinear form $a(\cdot,\cdot)$ is coercive on $\boldsymbol{V}_h(\operatorname{div}0)\times\boldsymbol{C}_h$.

By Schwarz's inequality, we find that, for any $\boldsymbol{\Psi}=(\boldsymbol{w},\boldsymbol{\psi})$ and $\boldsymbol{\Phi}=(\boldsymbol{v},\boldsymbol{\varphi})$,

$$|a(\boldsymbol{\Psi},\boldsymbol{\Phi})| \leq |||\boldsymbol{\Psi}|||\,|||\boldsymbol{\Phi}||| + |O_h(\boldsymbol{u}_*;\boldsymbol{w},\boldsymbol{v})|\,.$$

From Lemma 3.3 and 3.2, we have

$$|O_h(\boldsymbol{u}_*;\boldsymbol{w},\boldsymbol{v})| \leq C_0\big\|\boldsymbol{u}_*\big\|_{1,h}\left\|\boldsymbol{w}\right\|_{1,h}\left\|\boldsymbol{v}\right\|_{1,h} \leq C_0\theta_1^2R_e^{-2}\left\|\boldsymbol{u}_*\right\|_{1,h}\left\|\boldsymbol{w}\right\|_{\mathcal{A}_h}\left\|\boldsymbol{v}\right\|_{\mathcal{A}_h}.$$

This implies the continuity of $a(\cdot,\cdot)$, namely,

$$|a(\boldsymbol{\Psi},\boldsymbol{\Phi})| \leq \left(1+C_0\theta_1^2R_e^{-2}\left\|\boldsymbol{u}_*\right\|_{1,h}\right)|||\boldsymbol{\Psi}|||\,|||\boldsymbol{\Phi}|||\,.$$

By the Lax-Milgram lemma, the linear problem (3.10) has a unique solution. □

Remark 3.1. The discrete energy law can be understood similarly as in Remark 2.1. For the discrete scheme, the tangential discontinuity of the velocity also introduces a dissipative term due to upwinding.

Corollary 3.1. *There exists a constant $C>0$ depending only on physical parameters such that*

$$\mathsf{E}_m+\frac{1}{2}\sum_{n=1}^{m}\tau\mathsf{P}_n = \mathsf{E}_0 + C\sum_{n=1}^{m}\tau\left\|\boldsymbol{f}_n\right\|^2_{\boldsymbol{L}^2(\Omega)}, \quad 1\leq m\leq N.$$

Proof. From Theorem 3.1 we know that

$$\frac{\mathsf{E}_n-\mathsf{E}_{n-1}}{\tau}+\mathsf{P}_n = (\boldsymbol{f}_n,\bar{\boldsymbol{u}}_n) \qquad \forall\, n\geq 1.$$

Summing the above equality with respect to $n = 1, \cdots, m$, we have

$$\mathsf{E}_m + \sum_{n=2}^{m} \tau \mathsf{P}_n = \mathsf{E}_1 + \sum_{n=2}^{m} \tau(\boldsymbol{f}_n, \bar{\boldsymbol{u}}_n). \tag{3.11}$$

Similarly, by Lemma 3.1 and Lemma 3.2, we have

$$\begin{aligned} |(\boldsymbol{f}_n, \bar{\boldsymbol{u}}_n)| &\le \|\boldsymbol{f}_n\|_{\boldsymbol{L}^2(\Omega)} \|\bar{\boldsymbol{u}}_n\|_{\boldsymbol{L}^2(\Omega)} \le C \|\boldsymbol{f}_n\|_{\boldsymbol{L}^2(\Omega)} \|\bar{\boldsymbol{u}}_n\|_{\mathcal{A}_h} \\ &\le C \|\boldsymbol{f}_n\|^2_{\boldsymbol{L}^2(\Omega)} + \frac{1}{2} \|\bar{\boldsymbol{u}}_n\|^2_{\mathcal{A}_h}. \end{aligned}$$

Summing all the equalities with respect to $n = 2, \cdots, m$ yields

$$\sum_{n=2}^{m} \tau(\boldsymbol{f}_n, \bar{\boldsymbol{u}}_n) \le C \sum_{n=2}^{m} \tau \|\boldsymbol{f}_n\|^2_{\boldsymbol{L}^2(\Omega)} + \frac{1}{2} \sum_{n=2}^{m} \tau \mathsf{P}_n. \tag{3.12}$$

The proof is completed by inserting (3.12) into (3.11). □

Remark 3.2. In fact, Corollary 3.1 gives the stability of physical quantities

$$\begin{cases} \boldsymbol{u}_h(t) = l(t)\boldsymbol{u}_{n-1} + [1 - l(t)]\boldsymbol{u}_n, \\ \boldsymbol{B}_h(t) = l(t)\boldsymbol{B}_{n-1} + [1 - l(t)]\boldsymbol{B}_n, \qquad \forall\, t \in [t_{n-1}, t_n), \\ \boldsymbol{J}_h(t) = l(t)\boldsymbol{J}_{n-1} + [1 - l(t)]\boldsymbol{J}_n, \end{cases}$$

where $l(t) = (t_n - t)/\tau$ and $1 \le n \le N$. Suppose $\sum_{n=1}^{N} \tau \|\boldsymbol{f}_n\|^2_{\boldsymbol{L}^2(\Omega)} \le C$. We find that

$$\|\boldsymbol{u}_h\|^2_{\boldsymbol{L}^\infty(0,T;\boldsymbol{L}^2(\Omega))} + \|\boldsymbol{B}_h\|^2_{\boldsymbol{L}^\infty(0,T;\boldsymbol{H}(\mathrm{div},\Omega))} + \int_0^T \left[\|\boldsymbol{u}_h\|^2_{\mathcal{A}_h} + \|\boldsymbol{J}_h\|^2_{\boldsymbol{L}^2(\Omega)}\right] \mathrm{d}t \le C.$$

Therefore, we can extract convergent subsequences of $\boldsymbol{u}_h$, $\boldsymbol{B}_h$, and $\boldsymbol{J}_h$ as $\tau, h \to 0$. The convergence of the discrete solutions and the finite element error analysis will be our future work.

4. A preconditioner for the discrete problem

The purpose of this section is to propose a preconditioner for solving (3.6). Instead of solving $\bar{\boldsymbol{u}}_n$ in the divergence-free finite element space, we introduce a Lagrangian multiplier p_n and solve $\bar{\boldsymbol{u}}_n$ in the unconstrained space $\boldsymbol{V}_h$. In fact, p_n is a piecewise constant approximation of the pressure and will belong to the space

$$Q_h = \{q \in L^2_0(\Omega) : q|_K \in \mathbb{R},\ K \in \mathcal{T}_h\}.$$

For any $\boldsymbol{\Psi} = (\boldsymbol{u}, \boldsymbol{\psi})$, $\boldsymbol{\Phi} = (\boldsymbol{v}, \boldsymbol{\varphi})$ with $\boldsymbol{u}, \boldsymbol{v} \in \boldsymbol{V}_h$ and $\boldsymbol{\psi}, \boldsymbol{\varphi} \in \boldsymbol{C}_h$, define

$$a_1(\boldsymbol{\Psi}, \boldsymbol{\Phi}) = a(\boldsymbol{\Psi}, \boldsymbol{\Phi}) + 2\tau^{-1}(\mathrm{div}\, \boldsymbol{u}, \mathrm{div}\, \boldsymbol{v}).$$

The resulting augmented version of (3.6) reads: Find $\boldsymbol{\Psi}_n \in \boldsymbol{V}_h \times \boldsymbol{C}_h$ and $p_n \in Q_h$ such that

$$a_1(\bar{\boldsymbol{\Psi}}_n, \boldsymbol{\Phi}) - (\mathrm{div}\, \boldsymbol{v}, p_n) = f(\boldsymbol{\Phi}) \qquad \forall\, \boldsymbol{\Phi} = (\boldsymbol{v}, \boldsymbol{\varphi}) \in \boldsymbol{V}_h \times \boldsymbol{C}_h, \tag{4.1a}$$

$$(\mathrm{div}\, \bar{\boldsymbol{u}}_n, q) = 0 \qquad \forall\, q \in Q_h. \tag{4.1b}$$

Since $\operatorname{div} \bar{\boldsymbol{u}}_n = 0$ from (4.1b), it holds actually

$$a_1(\bar{\boldsymbol{\Psi}}_n, \boldsymbol{\Phi}) = a(\boldsymbol{\Psi}_n, \boldsymbol{\Phi}) \qquad \forall\, \boldsymbol{\Phi} \in \boldsymbol{V}_h \times \boldsymbol{C}_h.$$

This yields the equivalence of (3.10) and (4.1). Hence, the term $2\tau^{-1}(\operatorname{div} \bar{\boldsymbol{u}}_n, \operatorname{div} \boldsymbol{v})$ does not effect the discrete solutions, but enhances the stability of the mixed formulation.

Clearly the linear problem (4.1) can be written into an algebraic form

$$\begin{pmatrix} \mathbb{F} & \mathbb{B}^\top & \mathbb{J}^\top \\ \mathbb{B} & 0 & 0 \\ \mathbb{J} & 0 & \mathbb{C} \end{pmatrix} \begin{pmatrix} \mathbf{x}_u \\ \mathbf{x}_p \\ \mathbf{x}_A \end{pmatrix} = \begin{pmatrix} \mathbf{b}_u \\ \mathbf{b}_p \\ \mathbf{b}_A \end{pmatrix}, \tag{4.2}$$

where $\mathbf{x}_u, \mathbf{x}_p, \mathbf{x}_A$ are vectors of DOFs belonging to $\bar{\boldsymbol{u}}_n$, p_n, $\bar{\boldsymbol{A}}_n$ respectively and $\mathbf{b}_u, \mathbf{b}_p, \mathbf{b}_A$ are the corresponding load vectors. Let $\mathbb{A}$ denote the stiffness matrix. Its sub-matrices $\mathbb{F}$, $\mathbb{B}$, $\mathbb{J}$, $\mathbb{C}$ are the Galerkin matrices for the fluid terms, the pressure term, the coupling between $\bar{\boldsymbol{u}}_n$ and $\bar{\boldsymbol{A}}_n$, and the magnetic potential terms respectively, namely,

$$\begin{aligned} \mathbb{F} &\sim a_1((\bar{\boldsymbol{u}}_n, 0), (\boldsymbol{v}, 0)), \qquad \mathbb{B} \sim -(\operatorname{div} \boldsymbol{v}, p_n), \\ \mathbb{C} &\sim a_1((0, \bar{\boldsymbol{A}}_n), (0, \boldsymbol{\varphi})), \quad \mathbb{J} \sim \frac{2\kappa}{\tau} (\boldsymbol{\varphi}, \boldsymbol{B}_* \times \bar{\boldsymbol{u}}_n). \end{aligned}$$

To construct a preconditioner for $\mathbb{A}$, we drop $\mathbb{J}$ and get

$$\mathbb{A} \sim \mathbb{A}_0 = \begin{pmatrix} \mathbb{F} & \mathbb{B}^\top & \mathbb{J}^\top \\ \mathbb{B} & 0 & 0 \\ 0 & 0 & \mathbb{C} \end{pmatrix}.$$

It suffices to study the preconditioner for the 2×2 Navier-Stokes block and the preconditioner for the Maxwell block $\mathbb{C}$ respectively.

Note that $\mathbb{C}$ is just the stiffness matrix of the Maxwell equation without advection. It can be preconditioned by the auxiliary space preconditioning method proposed in Ref. 17. For the Navier-Stokes block of the stiffness matrix, we consider the LU-decomposition

$$\begin{pmatrix} \mathbb{F} & \mathbb{B}^\top \\ \mathbb{B} & 0 \end{pmatrix} = \begin{pmatrix} \mathbb{I} & 0 \\ \mathbb{B}\mathbb{F}^{-1} & \mathbb{I} \end{pmatrix} \begin{pmatrix} \mathbb{F} & \mathbb{B}^\top \\ 0 & -\mathbb{B}\mathbb{F}^{-1}\mathbb{B}^\top \end{pmatrix}.$$

Inspired by Ref. 5, we approximate the Schur complement as follows

$$\mathbb{B}\mathbb{F}^{-1}\mathbb{B}^\top \approx \mathbb{Q}_p, \qquad \mathbb{Q}_p = \frac{\tau}{2} \left(\int_\Omega q_i q_j \right),$$

where $2\tau^{-1}\mathbb{Q}_p$ is the mass matrix on the pressure finite element space and $\{q_i\}$ is the basis of Q_h. Therefore, we can choose the right matrix of the LU-decomposition as a preconditioner of the Navier-Stokes block, namely,

$$\begin{pmatrix} \mathbb{F} & \mathbb{B}^\top \\ \mathbb{B} & 0 \end{pmatrix} \sim \begin{pmatrix} \mathbb{F} & \mathbb{B}^\top \\ 0 & -\mathbb{B}\mathbb{F}^{-1}\mathbb{B}^\top \end{pmatrix} \sim \begin{pmatrix} \mathbb{F} & \mathbb{B}^\top \\ 0 & -\mathbb{Q}_p \end{pmatrix}.$$

To summarize, we propose an iterative solver for (4.2). In each time step, the initial guess for $(\mathbf{x}_u, \mathbf{x}_p, \mathbf{x}_A)$ is chosen as the solution in the previous time step. Given an approximation $(\tilde{\mathbf{x}}_u, \tilde{\mathbf{x}}_p, \tilde{\mathbf{x}}_A)$ of $(\mathbf{x}_u, \mathbf{x}_p, \mathbf{x}_A)$, let $(\mathbf{e}_u, \mathbf{e}_p, \mathbf{e}_A)$ be the corrections for $(\tilde{\mathbf{x}}_u, \tilde{\mathbf{x}}_p, \tilde{\mathbf{x}}_A)$ and let $(\mathbf{r}_u, \mathbf{r}_p, \mathbf{r}_A)$ be the corresponding residual vectors. We present the algorithm for solving the residual equation

$$\begin{pmatrix} \mathbb{F} & \mathbb{B}^\top & \mathbb{J}^\top \\ 0 & -\mathbb{Q}_p & 0 \\ 0 & 0 & \mathbb{C} \end{pmatrix} \begin{pmatrix} \mathbf{e}_u \\ \mathbf{e}_p \\ \mathbf{e}_A \end{pmatrix} = \begin{pmatrix} \mathbf{r}_u \\ \mathbf{r}_p \\ \mathbf{r}_A \end{pmatrix}$$

Algorithm 4.1. The residual equation is solved in three steps:

(1) Solve $\mathbb{C}\mathbf{e}_A = \mathbf{r}_A$ by the CG method with the Hiptmair-Xu preconditioner (cf. Ref. 17) such that the relative residual is less than 10^{-3}.
(2) Solve $\mathbb{Q}_p\mathbf{e}_p = -\mathbf{r}_p$ by the CG method with diagonal preconditioner such that the relative residual is less than 10^{-3}.
(3) Solve $\mathbb{F}\mathbf{e}_u = \mathbf{r}_u - \mathbb{B}^\top\mathbf{e}_p - \mathbb{J}^\top\mathbf{e}_A$ by the GMRES method with the additive Schwarz preconditioner (cf. Ref. 7) such that the relative residual is less than 10^{-3}.

5. Numerical experiments

In this section, we confirm the prediction of the theory and demonstrate the robustness of the solver by four numerical experiments. Our implementation is based on the adaptive finite element package "Parallel Hierarchical Grid" (PHG) (cf. Ref. 32) and the computations are carried out on the cluster LSSC-III of the State Key Laboratory on Scientific and Engineering Computing, Chinese Academy of Sciences.

The first example is to show the efficiency of the solver for the linearly extrapolated scheme (3.6) compared with the nonlinear solver for the Crank-Nicolson scheme (3.3). The second example is to show the convergence rate of the fully discrete scheme. The third example is to demonstrate the optimality of the preconditioner with respect to the number of DOFs and the robustness of the preconditioner for relatively large parameters. The fourth example is the benchmark problem for a three-dimensional driven cavity flow. With this example, we validate the $\boldsymbol{A}$-based MHD formulation and demonstrate the robustness of the preconditioner. In both examples, we set the penalty parameter to $\alpha = 10$ and use the computational domain $\Omega = (0, 1)^3$.

Example 5.1. This example is to confirm the efficiency of the linearly extrapolated scheme (3.6) compared with the nonlinear Crank-Nicolson scheme (3.3). The physical parameters are given by $R_e = R_m = \kappa = 1$ and the terminal time $T = 1$. The right-hand sides and the Dirichlet boundary conditions are chosen so that the true solutions are given by

$$\boldsymbol{u} = \left(ye^{-t}, z\cos t, x\right), \quad p = 0, \quad \boldsymbol{A} = \left(z, 0, y\cos t\right).$$

Note that the exact solutions are linear in space. The approximate errors mainly come from the discretization of the time variable. We fix a tetrahedral mesh with $h = 0.433$ and test the convergence rate with respect to the time step size. In each time step, if we choose the initial guess by $\bar{\boldsymbol{u}}_n = \boldsymbol{u}_{n-1}$ and $\bar{\boldsymbol{A}}_n = \boldsymbol{A}_{n-1}$ and use *only one* nonlinear iteration, the Crank-Nicolson (C-N) scheme (3.3) will yield a first-order approximation to the continuous problem, while the linearly extrapolated scheme (3.6) is second-order. Let the approximation errors at the final time $t = T$ be denoted by

$$\boldsymbol{e}_u = \boldsymbol{u}(T) - \boldsymbol{u}_N, \quad e_p = p(T) - p_N, \quad \boldsymbol{e}_A = \boldsymbol{A}(T) - \boldsymbol{A}_N.$$

We set the tolerance for solving linear systems of equations to $\varepsilon = 10^{-10}$. Table 1 shows that the convergence rate for the C-N scheme with one Picard iteration is first-order, namely,

$$\|\boldsymbol{e}_u\|_{1,h} \sim \tau, \qquad \|e_p\|_{L^2(\Omega)} \sim \tau, \qquad \|\boldsymbol{e}_A\|_{\boldsymbol{H}(\mathbf{curl},\Omega)} \sim \tau.$$

Table 2 shows that the second-order convergence is obtained for the linearly extrapolated scheme

$$\|\boldsymbol{e}_u\|_{1,h} \sim \tau^2, \qquad \|e_p\|_{L^2(\Omega)} \sim \tau^2, \qquad \|\boldsymbol{e}_A\|_{\boldsymbol{H}(\mathbf{curl},\Omega)} \sim \tau^2.$$

Table 1. Convergence rates for the C-N scheme at $t = T$ with $m = 1$ and $\varepsilon = 10^{-10}$ (Example 5.1).

τ	$\|\boldsymbol{e}_u\|_{1,h}$	order	$\|e_p\|_{L^2}$	order	$\|\boldsymbol{e}_A\|_{\boldsymbol{H}(\mathbf{curl})}$	order	$\|\operatorname{div} \boldsymbol{u}_h\|_{L^2}$
0.200	7.99e-4	–	9.40-3	–	9.62e-3	–	1.51e-8
0.100	3.79e-4	1.08	1.71e-2	-0.86	5.03e-3	0.94	2.84e-9
0.050	1.90e-4	1.00	8.46e-3	1.02	2.56e-3	0.97	1.15e-9
0.025	9.47e-5	1.00	4.21e-3	1.00	1.29e-3	0.99	1.47e-10

Table 2. Convergence rates for the linearly extrapolated scheme at $t = T$. (Example 5.1).

τ	$\|\boldsymbol{e}_u\|_{1,h}$	order	$\|e_p\|_{L^2}$	order	$\|\boldsymbol{e}_A\|_{\boldsymbol{H}(\mathbf{curl})}$	order	$\|\operatorname{div} \boldsymbol{u}_h\|_{L^2}$
0.200	1.74e-4	–	2.71e-3	–	1.5e-3	–	1.53e-8
0.100	2.40e-5	2.86	1.09e-3	1.31	3.97e-4	1.92	3.79e-9
0.050	5.14e-6	2.22	2.70e-4	2.01	1.02e-4	1.96	1.83e-9
0.025	1.29e-6	1.99	6.69e-5	2.01	2.58e-5	1.98	2.74e-10

In fact, second-order convergence can be obtained for the C-N scheme by multiple Picard iterations, but with higher computational cost. To save computing time, we set the tolerance for solving linear systems of equations to $\varepsilon = 10^{-5}$. Table 3–5 show the convergence rates for the C-N schemes with $m = 2, 3, 4$ iterations respectively. Clearly we also get the second-order convergence for $m = 3, 4$.

Table 3. Convergence rates for the C-N scheme at the final time with $m = 2$ (Example 5.1).

τ	$\|\boldsymbol{e}_u\|_{1,h}$	order	$\|e_p\|_{L^2}$	order	$\|\boldsymbol{e}_A\|_{\boldsymbol{H}(\mathbf{curl})}$	order	$\|\mathrm{div}\,\boldsymbol{u}_h\|_{L^2}$
0.200	1.47e-4	–	8.60-4	–	8.20e-4	–	4.60e-7
0.100	5.54e-5	1.41	4.81e-4	0.84	2.79e-4	1.56	2.69e-7
0.050	1.86e-5	1.57	1.31e-4	1.88	9.25e-5	1.59	2.15e-8
0.025	5.71e-6	1.70	3.51e-5	1.90	3.02e-5	1.61	2.93e-9

Table 4. Convergence rates for the C-N scheme at the final time with $m = 3$ (Example 5.1).

τ	$\|\boldsymbol{e}_u\|_{1,h}$	order	$\|e_p\|_{L^2}$	order	$\|\boldsymbol{e}_A\|_{\boldsymbol{H}(\mathbf{curl})}$	order	$\|\mathrm{div}\,\boldsymbol{u}_h\|_{L^2}$
0.200	7.63e-5	–	7.36e-4	–	7.49e-4	–	1.87e-8
0.100	1.78e-5	2.10	4.43e-4	0.78	2.07e-4	1.86	8.22e-9
0.050	4.44e-6	2.00	1.12e-4	1.98	5.33e-5	1.96	5.47e-10
0.025	1.13e-6	1.97	2.80e-5	2.00	1.35e-5	1.98	3.85e-11

Table 5. Convergence rates for the C-N scheme at the final time with $m = 4$ (Example 5.1).

τ	$\|\boldsymbol{e}_u\|_{1,h}$	order	$\|e_p\|_{L^2}$	order	$\|\boldsymbol{e}_A\|_{\boldsymbol{H}(\mathbf{curl})}$	order	$\|\mathrm{div}\,\boldsymbol{u}_h\|_{L^2}$
0.200	7.60e-5	–	7.29e-4	–	7.44e-4	–	9.60e-10
0.100	1.77e-5	2.10	4.40e-4	0.73	2.05e-4	1.86	3.35e-10
0.050	4.40e-6	2.01	1.11e-4	1.99	5.29e-5	1.95	1.26e-11
0.025	1.11e-6	1.99	2.79e-5	1.99	1.34e-5	1.98	1.22e-11

To test the relative efficiency of the linear scheme to the nonlinear scheme, we compare both the errors and the computing time for $T = 10$. We choose $\tau = 1/80$, $\varepsilon = 10^{-10}$ for the linearly extrapolated scheme and $\tau = 1/40$, $\varepsilon = 10^{-5}$ for the Crank-Nicolson scheme. We use $m = 2, 3$ Picard iterations for the nonlinear solver respectively. Table 6 shows that the linearly extrapolated scheme is more efficient for long-time simulations.

Table 6. The extrapolated scheme and the C-N scheme with m Picard iterations ($T = 10$).

Schemes	τ	Time (s)	$\|\boldsymbol{e}_u\|_{1,h}$	$\|e_p\|_{L^2(\Omega)}$	$\|\boldsymbol{e}_A\|_{\boldsymbol{H}(\mathbf{curl},\Omega)}$
linear	1/80	2842	1.05e-6	1.92e-5	3.41e-5
C-N ($m = 2$)	1/40	2877	3.78e-6	6.44e-4	9.92e-5
C-N ($m = 3$)	1/40	4266	1.46e-6	2.62e-5	9.36e-5

Example 5.2. This example is to test the convergence rate for the linearly extrapolated scheme where both the time step size and the mesh size are refined

simultaneously. The physical parameters are given by $R_e = R_m = \kappa = 1$ and the terminal time $T = 0.2$. The right-hand sides and the Dirichlet boundary conditions are chosen so that the true solutions are given by

$$\boldsymbol{u} = (\sin t \sin y, 0, 0)\,, \quad p = x + y + z - 1.5, \quad \boldsymbol{A} = (0, \sin(t + x), 0)\,.$$

We set the time step size by $\tau_0 = 0.05$ and the mesh size by $h_0 = 0.866$ initially and then bisect them successively. Table 7 shows the errors at the final time T. Asymptotically, we find that

$$\|\boldsymbol{e}_u\|_{\boldsymbol{L}^2(\Omega)} \sim O(\tau^2 + h^2),\ \|\boldsymbol{e}_A\|_{\boldsymbol{L}^2(\Omega)} \sim O(\tau^2 + h^2),$$
$$|\boldsymbol{e}_u|_{1,h} \sim O(\tau^2 + h), \qquad \|\boldsymbol{e}_A\|_{\boldsymbol{H}(\mathbf{curl},\Omega)} \sim O(\tau^2 + h),\ \|e_p\|_{L^2(\Omega)} \sim O(\tau^2 + h).$$

Table 7. Optimal convergence in $\boldsymbol{L}^2(\Omega)$ norms (Example 5.2).

(τ, h)	$\|\boldsymbol{e}_u\|_{L^2}$	$\|\boldsymbol{e}_u\|_{1,h}$	$\|e_p\|_{L^2}$	$\|\boldsymbol{e}_A\|_{L^2}$	$\|\boldsymbol{e}_A\|_{\boldsymbol{H}(\mathbf{curl})}$
(τ_0, h_0)	7.6e-4	1.3e-2	1.8e-1	1.0e-2	7.5e-2
$(\tau_0, h_0)/2$	1.9e-4	6.2e-3	8.9e-2	2.7e-3	3.7e-2
$(\tau_0, h_0)/4$	4.9e-5	3.0e-3	4.4e-2	6.9e-4	1.8e-2
$(\tau_0, h_0)/8$	1.3e-5	1.5e-3	2.2e-2	1.7e-4	9.1e-3

Example 5.3. This example is to test the optimality of the preconditioner given by Algorithm 4.1 with respect to the number of DOFs. We also show the robustness of the preconditioner for relatively large physical parameters and for large time step size. Here we set $R_e = R_m = 100$, $\kappa = 10$ and choose $\tau = 0.1$, $T = 1$.

The initial conditions and the right-hand side are given respectively by

$$\boldsymbol{u}_0 = \left(2y - 2yx^2, 2x - 2xy^2, 0\right), \qquad \boldsymbol{A}_0 = (y, 0, 0), \qquad \boldsymbol{f} = 0.$$

This gives the initial magnetic field $\boldsymbol{B}_0 = (0, 0, 1)$. The boundary conditions are

$$\boldsymbol{u} = \boldsymbol{u}_0, \quad \boldsymbol{A} \times \boldsymbol{n} = \boldsymbol{A}_0 \times \boldsymbol{n} \quad \text{on } \Omega.$$

Table 8 shows the number of GMRES iterations, N_{it}, to reduce the residual of the algebraic system by a factor $\varepsilon = 10^{-10}$. Clearly N_{it} is uniform with respect to h.

Table 8. Optimality of the preconditioned GMRES algorithm (Example 5.3).

h	N_{it}	DOFs for $\boldsymbol{u}_n$	DOFs for p_n	DOFs for $\boldsymbol{A}_n$
0.866	12	3.6e+2	4.8e+1	2.0e+2
0.433	12	2.6e+3	3.8e+2	1.2e+3
0.216	12	2.0e+4	3.1e+3	8.4e+3
0.108	12	1.5e+5	2.5e+4	6.2e+4

Example 5.4 (Driven Cavity Flow). This example computes the benchmark problem of driven cavity flow. The right-hand side of the momentum equation is set by $\boldsymbol{f} = 0$. The initial values are given by $\boldsymbol{A}_0 = (0, 0, y)$, $\boldsymbol{u}_0 = (v, 0, 0)$ where $v \in C^1(\bar{\Omega})$ and satisfies

$$v(x, y, 1) = 1 \qquad \text{and} \qquad v(x, y, z) = 0 \quad \forall\, z \in [0, 1 - h].$$

The boundary conditions are set by

$$\boldsymbol{u} = \boldsymbol{u}_0, \quad \boldsymbol{A} \times \boldsymbol{n} = 0 \qquad \text{on } \partial\Omega.$$

The physical parameters are $R_e = 100, R_m = 200$ and $\kappa = 10$.

In this example, we use Nédélec's second-order edge elements of the second family to compute $\boldsymbol{A}_n$ which yield a better approximation to the magnetic induction Ref. 24. Moreover, to capture the boundary layer near the top and the bottom of the cavity, we refine the mesh locally there (see Fig. 1). The numbers of DOFs are $272,904$ for $\boldsymbol{u}_n$, $44,032$ for p_n, and $440,781$ for $\boldsymbol{A}_n$. The time step is $\tau = 0.01$. The terminal time T is so chosen that the physical fields reach steady state, namely,

$$\frac{\|\boldsymbol{u}_n - \boldsymbol{u}_{n-1}\|_{\boldsymbol{L}^2(\Omega)}}{\|\boldsymbol{u}_n\|_{\boldsymbol{L}^2(\Omega)}} + \frac{\|\boldsymbol{A}_n - \boldsymbol{A}_{n-1}\|_{\boldsymbol{L}^2(\Omega)}}{\|\boldsymbol{A}_n\|_{\boldsymbol{L}^2(\Omega)}} + \frac{\|p_n - p_{n-1}\|_{L^2(\Omega)}}{\|p_n\|_{L^2(\Omega)}} < 10^{-8}.$$

The tolerance for the relative residual of the GMRES method is set by $\varepsilon = 10^{-10}$. Fig 2 shows the convergence of the preconditioned GMRES method with respect to the number of iterations at the final time $T = 3.98$. It takes only 10 iterations to reduce the relative residual below ε.

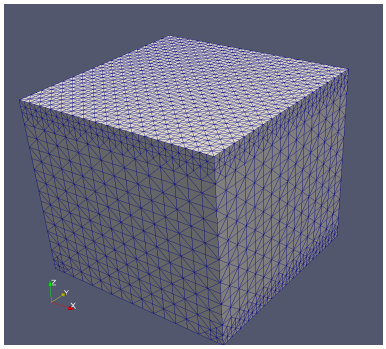

Fig. 1. A tetrahedral mesh with $44,032$ elements.

The left figure of Fig 3 shows the streamlines of fluid projected onto the cross section $y = 0.5$ and the right one shows the 2D simulation in Ref. 20 where Maxwell's equations are replaced with Poisson's equation for the electric potential. Our 3D results show clearly the flow of the fluid from the upper vortex to the lower vertex.

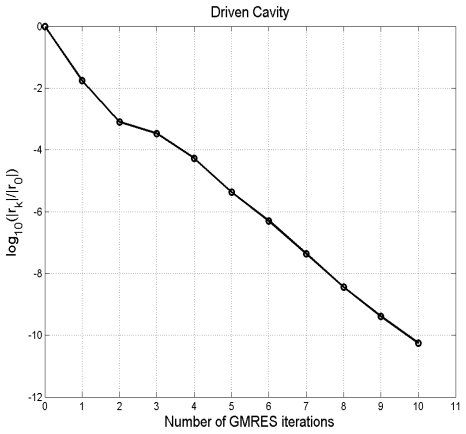

Fig. 2. Number of GMRES iterations for reducing the relative residual below 10^{-10}.

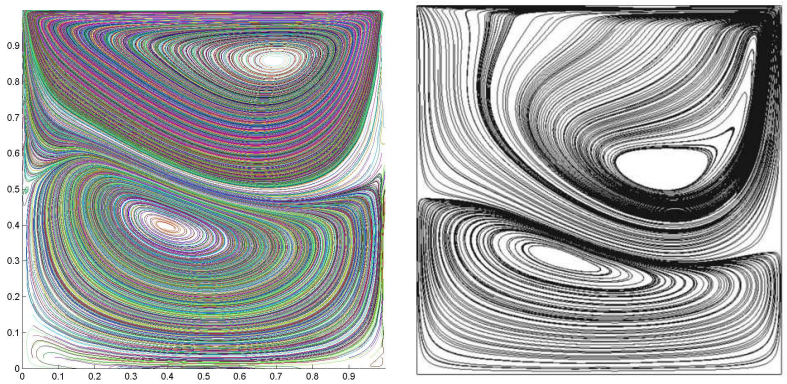

Fig. 3. Projection of the streamlines on the cross section $y = 0.5$

Fig. 4 shows the variation of the fluid kinetic energy $\mathsf{E}_{\mathrm{kin}}$, the magnetic field energy $\mathsf{E}_{\mathrm{mag}}$, and total energy $\mathsf{E} = \mathsf{E}_{\mathrm{kin}} + \mathsf{E}_{\mathrm{mag}}$ with respect to time, where

$$\mathsf{E}_{\mathrm{kin}} = \frac{1}{2} \|\boldsymbol{u}_n\|^2_{\boldsymbol{L}^2(\Omega)} , \qquad \mathsf{E}_{\mathrm{mag}} = \frac{\kappa}{2R_m} \|\mathbf{curl}\, \boldsymbol{A}_n\|^2_{\boldsymbol{L}^2(\Omega)} .$$

When the fluid tends to be steady, the total energy and the two portions of the total energy become invariant in time.

Fig. 5 shows the distribution of the kinetic pressure on three cross sections $x = 0.5$, $y = 0.5$, and $z = 0.5$ respectively. In the middle figure, since the flow is driven from left to right, it generates high pressure regions near the left and the right upper corners. Fig. 6 shows magnetic lines of $\boldsymbol{B}_n$ on the cross section $x = 0.5$ and the cross section $y = 0.5$ respectively. Fig. 7 shows the eddy current density $\boldsymbol{J}_n$ on the cross section $x = 0.5$ and the cross section $z = 0.5$ respectively. They tells us how the fluid influences the electromagnetic fields.

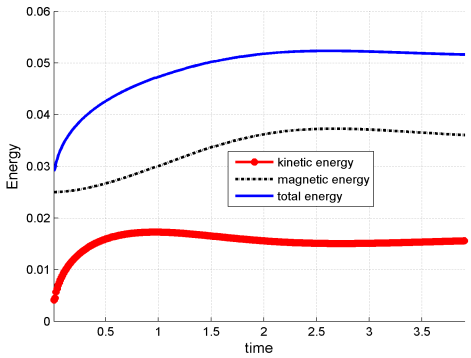

Fig. 4. Variance of fluid kinetic energy, magnetic field energy, and total energy in time.

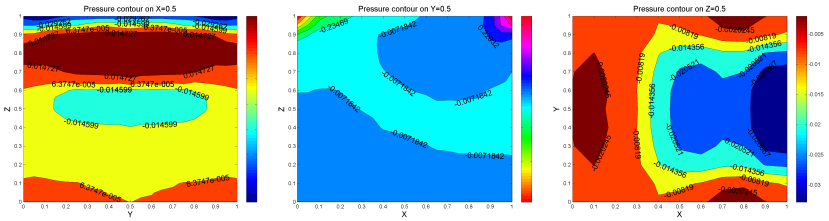

Fig. 5. Pressure contours on three cross sections $x = 0.5$, $y = 0.5$, and $y = 0.5$.

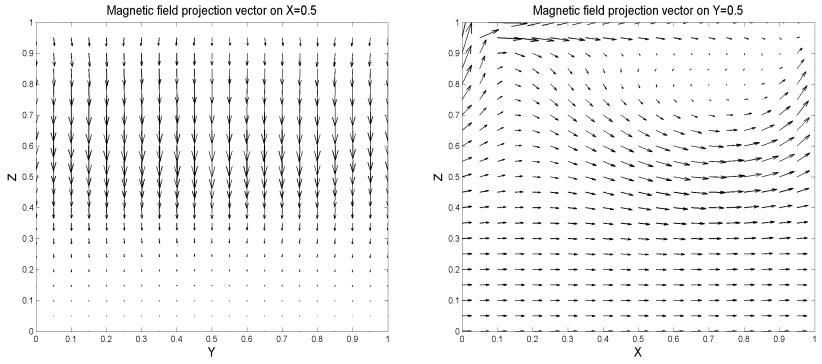

Fig. 6. Projection of $\boldsymbol{B}_n$ onto two cross sections $x = 0.5$ (left) and $y = 0.5$ (right).

Acknowledgment

This work is supported in part by the National Center for Mathematics and Interdisciplinary Sciences of China, the State Key Laboratory of Scientific and Engineering Computing of China, and National Magnetic Confinement Fusion Science Program of China (2015GB110003). S. Mao is supported by the National Key Research and Development Program of China (2016YFB0201304), China NSF 11471329, and

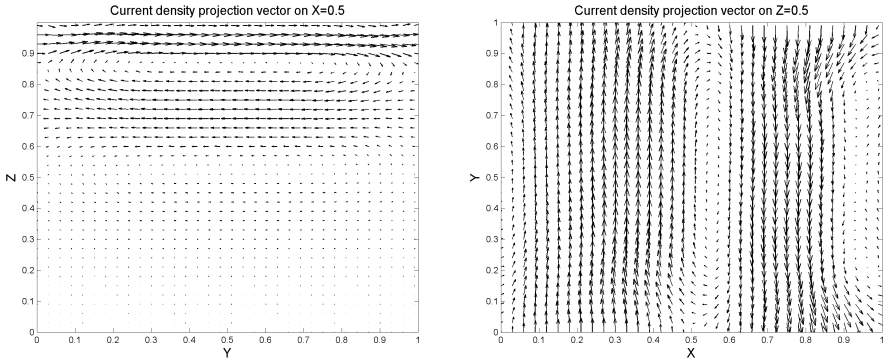

Fig. 7. Projection of $\boldsymbol{J}_n$ onto two cross sections $x = 0.5$ (left) and $z = 0.5$ (right).

Youth Innovation Promotion Association of CAS (2016003). W. Zheng is supported by China NSF under the grant 91430215.

References

1. M.A. Abdou et al., On the exploration of innovative concepts for fusion chamber technology fusion, *Fusion Eng. Des.* **54** (2001), 181-247.
2. M.A. Abdou et al., US Plans and strategy for ITER blanket testing, *Fusion Sci. Tech.* **47** (2005), 475-487.
3. F. Armero and J.C. Simo, Long-term dissipativity of time-stepping algorithms for an abstract evolution equation with applications to the incompressible MHD and Navier-Stokes equations, *Comput. Methods Appl. Mech. Engrg.* **131** (1996), 41-90.
4. D.N. Arnold, An interior penalty finite element method with discontinuous elements, *SIAM J. Numer. Anal.* **19** (1982), 742–760.
5. M. Benzi and M.A. Olshanskii, Field-of values convergence analysis of augmented Lagrangian preconditioners for the linearized Navier-Stokes problem, *SIAM J. Numer. Anal.* **49** (2011), 770-788.
6. S. Brenner, Poincaré-Friedrichs inequalities for piecewise H^1 functions, *SIAM J. Numer. Anal.* **41** (2003), 306-324.
7. X. Cai and M. Sarkis, A restricted additive Schwarz preconditioner for general sparse linear systems, *SIAM J. Sci. Comput.* **21** (1999), 792–797.
8. B. Cockburn, G. Kanschat, and D. Schötzau, A locally conservative LDG method for the incompressible Navier-Stokes equations, *Math. Comp.* **74** (2004), 1067-1095.
9. J.F. Gerbeau, A stabilized finite element method for the incompressible magnetohydrodynamic equations, *Numer. Math.* **87** (2000), 83–111.
10. V. Girault, B. Riviére, and M.F. Wheeler, *Finite element methods for Navier-Stokes Equations* (Springer-Verlag, 1986).
11. V. Girault, B. Riviére, and M.F. Wheeler, A discontinuous Galerkin method with nonoverlapping domain decomposition for the stokes and Navier-Stokes problems, *Math. Comp.* **74** (2004), 53–84.
12. C. Greif, D. Li, D. Schötzau, and X. Wei, A mixed finite element method with exactly divergence-free velocities for incompressible magnetohydrodynamics, *Comput. Methods Appl. Mech. Engrg.* **199** (2010), 2840-2855.
13. J.L. Guermond and P. Minev, Mixed finite element approximation of an MHD problem

involving conducting and insulating regions: the 3D case, *Numer. Meth. Part. Diff. Eqns.* **19** (2003), 709–731.
14. M.D. Gunzburger, A.J. Meir, and J.S. Peterson, On the existence and uniqueness and finite element approximation of solutions of the equations of stationary incompressible magnetohydrodynamics, *Math. Comp.* **56** (1991), 523–563.
15. P. Hansbo and M.G. Larson, Discontinuous Galerkin methods for incompressible and nearly incompressible elasticity by Nitsche's method, *Comput. Methods Appl. Mech. Engrg.* **191** (2002), 1895–1908.
16. R. Hiptmair, Finite elements in computational electromagnetism, *Acta Numerica* **11** (2002), 237–339.
17. R. Hiptmair and J. Xu, Nodal auxiliary space preconditioning in $\boldsymbol{H}(\mathbf{curl})$ and $\boldsymbol{H}(\mathrm{div})$ spaces, *SIAM J. Numer. Anal.* **45** (2007), 2483–2509.
18. K. Hu, Y. Ma, and J. Xu, Stable finite element methods preserving $\nabla \cdot \boldsymbol{B} = 0$ exactly for MHD models, *Numer. Math.* **135** (2017), 371-396.
19. Y. Ma, K. Hu, X. Hu, and J. Xu, Robust preconditioners for incompressible MHD models, *J. Comput. Phys.* **316** (2016), 721–746.
20. L. Marioni, F. Bay, and E. Hachem, Numerical stability analysis and flow simulation of lid-driven cavity subjected to high magnetic field, *Phys. Fluids* **28** (2016), 057102.
21. K.A. Mardal and R. Winther, Preconditioning discretizations of systmes of partial differential equations, *Numer Linear Algebra Appl.* **18** (2011), 1–40.
22. P. Monk, *Finite Element Methods for Maxwells Equations* (Oxford University Press, 2003).
23. R. Moreau, *Magnetohydrodynamics* (Kluwer Academic Publishers, 1990).
24. J.C. Nédélec, A new family of mixed finite elements in $\mathbb{R}^3$, *Numer. Math.* **50** (1986), 57–81.
25. M.-J. Ni, R. Munipalli, P. Huang, N.B. Morley, M.A. Abdou, A current density conservative scheme for incompressible MHD flows at a low magnetic Reynolds number. Part I. On a rectangular collocated grid system, *J. Comp. Phys.* **227** (2007), 174–204.
26. M.-J. Ni, R. Munipalli, P. Huang, N.B. Morley, M.A. Abdou, A current density conservative scheme for incompressible MHD flows at a low magnetic Reynolds number. Part II: On an arbitrary collocated mesh, *J. Comp. Phys.* **227** (2007), 205–228.
27. D. Schötzau, Mixed finite element methods for stationary incompressible magnetohydrodynamics, *Numer. Math.* **96** (2004), 771–800.
28. J. Xin, W. Cai, and N. Guo, On the construction of well-conditioned hierarchical bases for $\boldsymbol{H}(\mathrm{div})$-conforming $\mathbb{R}^n$ simplicial elements, *Commun. Comput. Phys.* **14** (2013), 621–638.
29. S.J. Xu, N.M. Zhang, and M.J. Ni, Influence of flow channel insert with pressure equalization opeing on MHD flows in a rectangular duct, *Fusion Eng. Des.* **88** (2013), 271–275.
30. Y. Zhang, Y. Hou, and L. Shan, Numerical analysis of the Crank-Nicolson extrapolation time discrete scheme for magnetohydrodynamics flows, *Numer. Methods Partial Differential Equations* **31** (2015), 2169–2208.
31. J. Zhang and M.J. Ni, A consistent and conservative scheme for MHD flows with complex boundaries on an unstructured Cartesian adaptive system, *J. Comp. Phys.* **256** (2014) 520–542.
32. L. Zhang, A parallel algorithm for adaptive local refinement of tetrahedral meshes using bisection, *Numer. Math.: Theor. Method Appl.* **2** (2009), 65–89. (http://lsec.cc.ac.cn/phg)